A STATISTICAL VLBI STUDY OF MILLI-ARCSECOND CORES IN EXTRAGALACTIC RADIO SOURCES

ROBERT A. PRESTON AND DAVID D. MORABITO
Jet Propulsion Laboratory, California Institute of Technology

AND

DAVID L. JAUNCEY
Division of Radiophysics, Commonwealth Scientific and Industrial Research Organization, Sydney, Australia
Received 1981 December 4; accepted 1982 December 3

ABSTRACT

VLBI observations at 2.3 GHz have been performed with a baseline of $\sim 8 \times 10^7$ wavelengths on a complete sample of 103 sources from the Parkes $\pm 4°$ catalog. Compact milli-arcsecond cores were found in 35% of all sources: 80% of quasars, only 10% of galaxies, and 20% of empty field sources. Virtually all of the sources appear to be at least partially resolved. For quasars, the percentage of the source flux density found to be coming from milli-arcsecond cores increased with increasing radio spectral index ($S \equiv kf^\alpha$), radio variability, and optical redness. Quasars with extended radio structure ($\gtrsim 10''$) seem more likely to possess a detectable milli-arcsecond core than do extended radio galaxies. The absence of a strong correlation between quasar milli-arcsecond structure and redshift is evidence for a lack of strong physical evolution in quasars, a hypothesis which is in agreement with previous studies of the size evolution of both quasar large-scale radio structure and radio lobe hot spots.

Subject headings: galaxies: nuclei — galaxies: structure — interferometry — quasars — radio sources: galaxies — radio sources: general

I. INTRODUCTION

The energy source which powers radio quasars or radio galaxies is commonly argued to lie in the nuclei of these objects, with the energy transport occurring by relativistic beams (e.g., Blandford and Rees 1974). Such a hypothesis provides a means of explaining the apparent long lifetime of extended radio structure, where the lifetime of relativistic electrons is thought to be quite short owing to energy losses incurred by incoherent synchrotron radiation. Direct observational support for such repeated or continuous beaming of energy from radio source nuclei is exhibited not only by the presence of apparent radio, optical, and X-ray jets in some sources, but also by examples of the alignment of radio structure over size scales differing by factors as large as $\sim 10^6$ (e.g., Readhead, Cohen, and Blandford 1978). The actual mechanism of energy production in these nuclear sources is not well understood, but an increasingly popular explanation is that the energy is produced by the loss of gravitational energy from matter spiraling into a black hole of up to $\sim 10^{10}$ solar masses with relativistic jets emerging from the nucleus along low-resistance paths perpendicular to the accretion disk.

To obtain a detailed understanding of the role of these nuclei in the energetics and evolution of extragalactic radio sources, it is important to conduct statistical investigations into the occurrence and properties of nuclei. Connected-element radio interferometers have been used for statistical studies of such nuclei at arc second resolution (e.g., Speed and Warwick 1978; Ulvestad *et al.* 1981). To probe closer to the source of the energy generation in radio source nuclei, the higher resolution capability of very long baseline interferometry (VLBI) is necessary. Pearson and Readhead (1981) have initiated a study to make VLBI maps of a complete sample of 51 radio sources at 5 GHz, but most VLBI studies to date have concentrated on the detailed compact structure of only a few radio sources. However, Broderick and Condon (1975) have used limited structure information to perform a statistical VLBI study at 430 MHz of a complete sample of 100 radio sources with minimum fringe spacings of $0''.06$. Schilizzi (1976) has used VLBI at 8.1 GHz to investigate the frequency of occurrence of compact nuclei in 39 radio galaxies with minimum fringe spacings of $0''.03$. In the present paper, we use a complete sample of 103 extragalactic radio sources to examine the statistical properties of compact nuclei at 2.3 GHz with fringe spacings of $0''.003$ and, hence, probe finer size scales than have previous statistical VLBI studies.

II. OBSERVATIONS AND DATA REDUCTION

The statistically complete sample of sources chosen for observations contains all 103 sources with 2.7 GHz

total flux density ≥ 0.5 Jy in the Parkes $\pm 4°$ catalog (Wall, Shimmins, and Merkelijn 1971) between 8 and 17 hours of right ascension. This catalog is useful for statistical studies because of the detailed information available on optical identifications, radio spectra, redshifts, radio variability, optical magnitude, optical color, and extended radio structure. The source positions were taken from McEwan, Browne, and Crowther (1975), and in most cases the errors are less than a few arc seconds.

The VLBI observations were performed at 2.29 GHz with right-circular polarization on a baseline between NASA Deep Space Stations at Goldstone, California (DSS 13), and at Tidbinbilla, Australia (DSS 43). The baseline length was 1.06×10^4 km, or 8.1×10^7 wavelengths. The data were gathered in seven separate observing sessions during 1977. At least two observations of 2 minutes duration were performed for all but four sources, with all cases of multiple observations providing consistent results. Because of the limited baseline rotation available with such widely separated antennas, the observations all occur at nearly the same (u, v)-values with a fringe spacing of about 2.6×10^{-3} arc seconds along a position angle of about 46°. With this interferometer, the normalized fringe visibility of a Gaussian source varies from 0.9 to 0.1 as the half-intensity diameter increases from $0\rlap{.}''4 \times 10^{-3}$ to $1\rlap{.}''7 \times 10^{-3}$. The brightness temperatures corresponding to these fringe visibilities are, respectively, 1.2×10^{12} K and 6×10^{10} K multiplied by the 2.3 GHz correlated flux density of the source in janskys.

National Radio Astronomy Observatory (NRAO) Mark II VLBI terminals were used to record the interferometric data (Clark 1973). Digital sampling and phase stability of the receiver chain were controlled by hydrogen-maser frequency standards. On-source system temperatures were measured at both antennas for each source so that the VLBI data could be properly calibrated.

Total flux density measurements were made for all sources at DSS 43. A noise-adding radiometer (Yerbury 1975) was used for gain stabilization as the antenna was scanned through each source. The overall uncertainty of the total flux density measurements is 2% with a noise and confusion error of 0.03 Jy. The Parkes 2.7 GHz corrections for angular size have been scaled to 2.3 GHz and applied where relevant.

Cross-correlation coefficients were obtained with the NRAO Mark II VLBI processor and postprocessor programs. To calculate correlated flux density, the coefficients were multiplied by the geometric mean of the system temperatures (K) of the two telescopes, by the geometric mean of the antenna sensitivities (Jy K^{-1}), and by a normalizing constant b, whose value was assumed to be 2.6 ± 0.2 as measured by Niell (1980, private communication). This b-value is consistent with our measured fringe visibilities, which reach but do not

exceed unity. Measurement of telescope sensitivities was performed during the experiments by system temperature measurements on calibration sources of known flux density (Klein and Stelzreid 1976).

The observations were broken into 1 minute segments, which set the rms noise level at ~ 0.02 Jy and the 5σ detection limit at ~ 0.1 Jy. However, uncertainties in detected source strength were dominated by calibration errors at about the 10% level. The major calibration uncertainty was the assumed 8% error in the estimate of the scaling constant b. Errors in antenna pointing are negligible. To ensure that no compact radio components would be missed because of source position errors, the sky was searched within $0\rlap{.}''5$ of all nominal source positions by cross-correlating over an appropriate range of delay and delay rate.

The results of the observations appear in Table 1.

III. DISCUSSION

a) The Detection of Milli-Arcsecond Cores as a Function of Optical Identification

Milli-arcsecond nuclei were detected in 36 out of 103 sources, or 35% of the sample. In the case of each detected source, only one milli-arcsecond component was found within the search radius of $0\rlap{.}''5$ from the nominal position (search resolution ~ 0.1). The distribution of detections and nondetections by optical identification is shown in Table 2. The optical identifications of the sample divide mainly into three similarly populated categories: quasars, galaxies, and empty fields. Outside these categories, four sources are classified as unidentified. The table shows that 78% (25 of 32) of the quasars, 10% (3 of 29) of the galaxies, and 18% (7 of 38) of empty field sources displayed detectable milli-arcsecond nuclei. It is interesting to compare these detection rates with those of Broderick and Condon (1975) in their 430 MHz VLBI study of a complete sample of 100 sources with 1400 MHz total flux densities > 2 Jy. Since their finding frequency is close to ours, the characteristics of their sample should be fairly similar to ours. With angular resolution 20 times coarser than ours and a detection limit 3 times smaller, they observed compact nuclei in 76% of the quasars and 14% of the galaxies. The similarity of the detection rates of quasars and galaxies in the two studies suggests that the compact nuclei in quasars and galaxies have increased in strength by approximately equal amounts from 430 MHz to 2.3 GHz, perhaps indicating that both types of objects are similar in nature with both being self-absorbed at 430 MHz.

The three galaxies detected in our observations all showed visibilities of ≤ 0.15 and correlated flux densities ≤ 0.3 Jy. A better determination of the frequency of occurrence of milli-arcsecond cores in radio galaxies requires more sensitive observations. We note that Schilizzi (1976) found $0\rlap{.}''01$ cores in 17 of 39 radio

TABLE 1
Observational Results

Source Name	Spectral Index[a]	Redshift[b]	Optl. ID[c]	Optl. Mag[d]	Color[e]	Var.[f]	Ang. Size[g]	Expt. Code[h]	Total Flux (Jy)	Correl. Flux (Jy)	Visibility[i]
P0803−00	−0.9	...	E4	15.9	1.6	...	34	B	0.87	< 0.12	< 0.14
								D		< 0.12	< 0.14
P0808+019 ...	0.2	...	Q	15.9	−0.2	V	...	B	0.39	0.28	0.72 ± 0.10
								D		0.32	0.82 ± 0.10
P0812+02	−0.7	0.402	Q	17.6	0.0	...	10	B	1.31	0.18	0.14 ± 0.02
								D		0.21	0.16 ± 0.02
P0812−02	−1.0	...	E1	19.3	1.9	...	...	B	1.21	< 0.12	< 0.10
								D		< 0.12	< 0.10
P0823+033 ...	0.2	...	Q	17.6	0.3	V	...	B	1.42	0.46	0.32 ± 0.04
								D		0.45	0.32 ± 0.03
P0828−03	−0.8	...	Q	19.8	0.1	...	...	B	0.65	< 0.12	< 0.19
								D		< 0.12	< 0.19
P0833−01	−0.7	...	E1	14.7	1.4	...	125	B	0.60	< 0.11	< 0.18
								D		< 0.12	< 0.20
P0837+035 ...	0.4	...	Q	21.1	...	...	...	B	0.65	< 0.11	< 0.17
								C		0.19	0.29 ± 0.05
P0850−03	−0.7	...	N2	19.2	2.1	...	...	B	0.90	< 0.12	< 0.13
								C		< 0.11	< 0.12
P0854−03	−0.6	...	N2	19.1	1.5	...	47	B	0.79	< 0.11	< 0.14
								C		< 0.11	< 0.14
P0906+01	−0.1	1.018	Q	17.6	0.0	V	...	A	0.76	0.11	0.15 ± 0.04
								B		0.13	0.17 ± 0.03
P0907−023 ...	−0.2	0.957	Q	18.8	0.1	...	...	A	0.53	< 0.11	< 0.21
								B		< 0.11	< 0.21
P0912+029 ...	−0.2	...	Q	20.1	0.1	V	...	A	0.68	0.53	0.78 ± 0.08
								B		0.56	0.82 ± 0.08
								C		0.54	0.79 ± 0.08
P0922+005 ...	0.2	1.720	Q	18.4	0.5	...	...	A	0.94	0.54	0.57 ± 0.06
								B		0.54	0.57 ± 0.07
P0932+02	−0.8	0.659	Q	17.6	−0.4	...	40	A	0.58	< 0.11	< 0.19
								B		< 0.11	< 0.19
P0938−01	−0.7	...	G	21.1	2.2	...	30	A	0.62	< 0.11	< 0.18
								B		< 0.11	< 0.18
P0940+02	−0.6	...	EF	...	...	...	10	A	0.96	< 0.11	< 0.12
								C		< 0.11	< 0.12
P0940+00	−0.7	...	EF	...	...	...	13	A	0.79	< 0.11	< 0.14
								C		< 0.11	< 0.14
P0949+00	−1.0	...	U	...	...	...	...	A	1.83	< 0.12	< 0.07
								B		< 0.12	< 0.07
P0955−01	−0.6	...	EF	...	...	...	...	A	0.83	< 0.11	< 0.13
								B		< 0.11	< 0.13
P0957+00	−0.9	0.907	Q	18.7	0.5	...	34	A	0.63	< 0.11	< 0.18
								B		< 0.11	< 0.18
P0958−001 ...	−1.0	...	EF	...	...	...	46	A	0.72	< 0.11	< 0.15
								B		< 0.11	< 0.15
P1004−018 ...	0.1	1.212	Q	19.8	0.7	...	...	A	0.64	0.24	0.38 ± 0.04
								B		0.27	0.42 ± 0.05
P1008−01	−0.6	...	U	...	...	V	135	A	0.92	0.18	0.20 ± 0.02
								D		< 0.11	< 0.12
P1021−00	0.3	2.547	Q	18.4	−0.1	...	...	A	0.92	< 0.11	< 0.12
								B		0.12	0.13 ± 0.01
								C		0.12	0.13 ± 0.02
P1027+00	−0.7	...	EF	...	...	...	...	A	0.69	< 0.11	< 0.16
								B		< 0.11	< 0.16
P1039+02	−0.6	...	EF	...	...	...	...	A	1.89	< 0.11	< 0.06
								B		< 0.11	< 0.06
P1046−02	−0.8	...	EF	...	...	...	40	A	0.60	< 0.11	< 0.18
								B		0.10	0.17 ± 0.03
P1054+004 ...	−0.4	...	EF	...	...	...	...	A	0.65	0.13	0.20 ± 0.03
								C		0.15	0.23 ± 0.03

TABLE 1—*Continued*

Source Name	Spectral Index[a]	Redshift[b]	Optl. ID[c]	Optl. Mag[d]	Color[e]	Var.[f]	Ang. Size[g]	Expt. Code[h]	Total Flux (Jy)	Correl. Flux (Jy)	Visibility[i]
P1055+01	−0.2	0.890	Q	18.7	0.7	...	...	A	2.87	1.34	0.47 ± 0.04
								C		1.38	0.48 ± 0.04
P1059−01	−0.9	...	EF	...	...	...	19	A	1.63	< 0.11	< 0.07
								C		< 0.12	< 0.07
P1059−023 ...	−0.9	...	EF	...	...	...	25	A	0.54	< 0.11	< 0.20
								C		< 0.11	< 0.20
P1103−006 ...	−0.7	0.426	Q	15.9	0.4	...	27	A	0.76	< 0.11	< 0.15
								C		< 0.11	< 0.15
P1106+023 ...	−0.5	...	NG	19.1	1.8	...	26	A	0.74	< 0.11	< 0.15
								C		< 0.11	< 0.15
P1110−01	−0.8	...	G	20.9	1.4	...	32	B	1.04	< 0.11	< 0.11
								C		< 0.11	< 0.11
P1115−023 ...	−0.7	...	G	20.6	1.1	...	24	C	0.68	< 0.11	< 0.16
P1116−02	−1.3	...	EF	...	...	...	...	A	0.76	< 0.11	< 0.15
								D		< 0.11	< 0.15
P1127+005 ...	−0.7	...	G	20.6	1.6	...	...	A	0.67	< 0.11	< 0.16
								C		< 0.11	< 0.16
P1130−037 ...	−0.7	...	E0	15.9	1.5	...	100	A	0.65	< 0.11	< 0.17
								C		< 0.11	< 0.17
P1132−000 ...	−0.6	...	EF	...	...	...	...	B	0.84	< 0.12	< 0.14
								C		< 0.11	< 0.13
P1134+01	−0.9	0.430	G	19.6	1.4	...	...	A	0.67	< 0.11	< 0.16
								C		< 0.11	< 0.16
P1138+01	−0.7	...	EF	...	...	...	...	A	1.82	< 0.11	< 0.06
								C		< 0.11	< 0.06
P1148−00	−0.1	1.982	Q	17.6	0.3	...	...	A	2.51	0.27	0.11 ± 0.01
								C		0.26	0.10 ± 0.01
P1212−00	−0.9	...	EF	...	...	...	...	A	0.71	< 0.11	< 0.16
								C		< 0.11	< 0.16
P1215+03	−0.9	0.077	E0	17.9	1.6	...	230	A	1.38	< 0.11	< 0.08
								C		< 0.11	< 0.08
P1218−02	−0.6	...	Q	19.	...	V	14	A	0.65	0.11	0.17 ± 0.05
								C		0.13	0.20 ± 0.03
								G		0.11	0.17 ± 0.05
P1222+037 ...	0.0	0.957	Q	19.8	0.6	V	...	A	0.96	0.93	0.97 ± 0.09
								C		0.96	1.00 ± 0.09
P1226+02	−0.2	0.158	Q	13.0	0.3	V	20	A	46.30	2.24	0.048 ± 0.004
								B		2.47	0.053 ± 0.004
								C		2.39	0.052 ± 0.004
								D		2.28	0.049 ± 0.004
								E		1.53	0.033 ± 0.003
								F		1.39	0.030 ± 0.003
P1229−02	−0.8	1.038	Q	17.1	−0.2	V	13	A	1.29	0.13	0.10 ± 0.02
								C		0.09	0.07 ± 0.02
P1249+035 ...	−0.7	...	E2	17.4	2.0	...	42	A	0.68	< 0.11	< 0.16
								C		< 0.11	< 0.16
P1250+029 ...	−0.8	...	G	20.6	2.6	...	14	A	1.10	< 0.11	< 0.10
								C		< 0.11	< 0.10
P1302−035 ...	−0.5	1.250	Q	20.1	0.6	V	...	A	0.75	0.16	0.21 ± 0.03
								D		0.13	0.17 ± 0.03
P1307+000 ...	−0.9	...	G	20.8	1.8	...	41	A	0.99	< 0.11	< 0.11
								G		< 0.13	< 0.13
P1317−00	−0.7	0.890	Q	18.8	0.5	...	...	A	1.12	0.10	0.09 ± 0.02
								C		< 0.11	< 0.10
P1317+019 ...	−0.2	...	Q	20.7	0.7	...	...	A	0.61	< 0.11	< 0.18
								C		0.06	0.10 ± 0.03
P1320+03	−0.8	...	G	20.0	1.8	...	53	A	0.88	< 0.11	< 0.13
								C		0.06	0.07 ± 0.02
P1325−01	−0.8	...	D	19.3	1.9	...	25	A	0.91	< 0.11	< 0.12
								C		< 0.11	< 0.12
P1330+02	−0.6	0.216	NG	18.9	0.9	...	63	A	2.03	0.19	0.09 ± 0.01
								C		0.18	0.09 ± 0.01
								G		0.20	0.07 ± 0.01

390

TABLE 1—*Continued*

Source Name	Spectral Index[a]	Redshift[b]	Optl. ID[c]	Optl. Mag[d]	Color[e]	Var.[f]	Ang. Size[g]	Expt. Code[h]	Total Flux (Jy)	Correl. Flux (Jy)	Visibility[i]
P1337−033 ...	−0.1	...	EF	...	...	...	...	A	0.75	0.30	0.40 ± 0.04
								C		0.30	0.40 ± 0.04
P1340+022 ...	−0.8	...	EF	...	...	...	...	A	0.60	< 0.11	< 0.18
								C		< 0.11	< 0.18
P1343−00	−0.7	...	EF	...	...	...	...	A	0.67	< 0.11	< 0.16
								C		< 0.11	< 0.16
P1349+027 ...	−0.5	...	EF	...	...	...	...	A	0.86	< 0.11	< 0.13
								C		< 0.11	< 0.13
P1351+021 ...	−0.1	1.606	Q	20.3	0.1	V	...	B	0.40	< 0.11	< 0.28
								C		< 0.11	< 0.28
P1351−018 ...	0.6	...	EF	...	...	V	...	A	0.84	0.67	0.80 ± 0.08
								C		0.62	0.74 ± 0.07
P1354+01	−0.8	...	EF	...	...	...	35	A	1.56	< 0.11	< 0.07
								C		< 0.11	< 0.07
P1355+01	−0.7	...	EF	...	...	...	9	A	1.22	< 0.11	< 0.09
								C		< 0.11	< 0.09
P1356+022 ...	−0.2	1.329	Q	18.7	0.5	V	...	A	0.79	0.45	0.57 ± 0.06
								C		0.40	0.51 ± 0.05
P1359+025 ...	−0.8	0.180	CG	19.0	1.7	...	23	A	0.72	< 0.11	< 0.15
								C		< 0.11	< 0.15
P1402−012 ...	0.6	2.518	Q	19.1	0.6	V	...	A	0.88	0.62	0.71 ± 0.07
								C		0.60	0.68 ± 0.06
P1404−01	−0.9	...	EF	...	...	...	37	A	0.73	< 0.11	< 0.15
								C		< 0.11	< 0.15
P1414−03	−0.9	...	EF	...	...	...	...	A	1.11	< 0.11	< 0.10
								C		< 0.11	< 0.10
P1425−01	−0.8	...	EF	...	...	...	12	A	1.85	< 0.11	< 0.06
								C		< 0.11	< 0.06
P1434+03	−0.5	...	EF	...	...	...	...	A	2.13	< 0.11	< 0.05
								C		< 0.11	< 0.05
P1446+00	−0.7	...	G	19.		...	14	A	1.16	< 0.11	< 0.10
								C		< 0.11	< 0.10
P1500−023 ...	−0.6	...	EF	...	...	...	...	A	0.61	< 0.11	< 0.18
								C		< 0.11	< 0.18
P1502+036 ...	0.0	0.411	Q	19.6	0.9	V	...	B	0.43	0.41	0.95 ± 0.11
								D		0.39	0.91 ± 0.11
P1503−001 ...	−0.7	...	G	19.5		...	25	D	0.64	< 0.11	< 0.17
								D		< 0.11	< 0.17
P1505+01	−0.9	...	EF	...	...	...	29	A	0.71	< 0.11	< 0.16
								D		< 0.11	< 0.16
P1509+022 ...	−0.6	0.219	CG	19.1	1.1	...	...	A	0.75	< 0.11	< 0.15
								D		< 0.11	< 0.15
P1509+01	−0.8	...	EF	...	...	...	11	A	1.46	< 0.11	< 0.08
								D		< 0.11	< 0.08
P1514+00	−0.5	0.053	E3	16.0	1.6	...	232	A	1.87	0.28	0.15 ± 0.02
								D		0.28	0.15 ± 0.02
P1523+03	−0.6	...	EF	...	...	...	...	A	1.35	< 0.11	< 0.08
								D		< 0.11	< 0.08
P1532+01	0.0	...	Q	19.8	0.8	V	...	A	1.19	0.56	0.47 ± 0.05
								D		0.56	0.47 ± 0.05
P1535+004 ...	0.5	...	EF	...	...	V	...	E	0.88	0.58	0.66 ± 0.06
								F		0.50	0.57 ± 0.05
P1543+01	−0.8	...	E	19.2	2.1	...	...	E	0.56	< 0.11	< 0.20
								F		< 0.11	< 0.20
P1543+005 ...	0.2	...	EF	...	...	...	...	E	1.18	0.20	0.17 ± 0.02
								F		0.19	0.16 ± 0.05
P1546+027 ...	0.2	0.412	Q	19.1	0.4	V	...	E	0.79	0.27	0.34 ± 0.04
								F		0.24	0.30 ± 0.04
P1555+001 ...	0.6	1.770	Q	20.2	1.1	V	...	D	2.42	2.06	0.85 ± 0.07
								E		2.45	1.01 ± 0.09
								F		2.26	0.93 ± 0.08
P1557−00	−0.1	...	EF	...	...	...	...	E	0.68	< 0.11	< 0.16
								F		< 0.11	< 0.16

TABLE 1—*Continued*

Source Name	Spectral Index[a]	Redshift[b]	Optl. ID[c]	Optl. Mag[d]	Color[e]	Var.[f]	Ang. Size[g]	Expt. Code[h]	Total Flux (Jy)	Correl. Flux (Jy)	Visibility[i]
P1559+02	−0.8	0.104	D	17.4	2.0	...	209	E	5.15	< 0.13	< 0.03
								F		< 0.12	< 0.02
P1602+01	−0.9	...	G	20.8	1.3	...	13	F	2.45	< 0.11	< 0.05
P1602−00	−0.8	1.625	Q	17.4	0.6	...	26	E	0.71	< 0.11	< 0.16
								F		< 0.11	< 0.16
P1603+005 ...	−0.9	...	U	...	...	...	...	E	0.78	< 0.11	< 0.14
								F		< 0.11	< 0.14
P1603+00	−0.6	...	E4	17.0	1.6	...	15	E	1.68	< 0.11	< 0.07
								F		< 0.11	< 0.07
P1615+029 ...	0.3	1.339	Q	17.6	−0.4	V	...	E	0.62	0.17	0.27 ± 0.04
								F		0.15	0.24 ± 0.05
P1635−035 ...	0.0	...	U	...	...	V	...	E	0.38	< 0.11	< 0.29
								F		< 0.11	< 0.29
P1638−025 ...	−0.7	...	EF	...	...	...	...	F	1.20	< 0.11	< 0.09
P1643+022 ...	−0.8	...	E2	18.2	1.7	...	10	E	1.31	< 0.11	< 0.08
								F		< 0.11	< 0.08
P1645+027 ...	−1.0	...	EF	...	...	...	...	E	0.61	< 0.11	< 0.18
								F		< 0.11	< 0.18
P1648+015 ...	−0.5	...	EF	...	...	...	...	E	0.54	0.42	0.78 ± 0.10
								F		0.38	0.70 ± 0.08
P1649−039 ...	−0.3	...	EF	...	...	...	56	E	0.53	< 0.11	< 0.21
								F		< 0.11	< 0.21
P1650+004 ...	−0.8	...	EF	...	...	...	...	E	0.81	< 0.11	< 0.14
								F		< 0.11	< 0.14
P1654−020 ...	−0.5	...	EF	...	...	...	...	E	0.67	< 0.11	< 0.16
								F		< 0.11	< 0.16

[a] Spectral indices (α_{318}^{2700}) are from Condon and Jauncey 1974 for sources north of −2° declination and from Wall 1972a for sources south of −2° declination (α_{178}^{2700}).

[b] Redshifts are from McEwan, Browne, and Crowther 1975, Wills and Lynds 1978, Burbidge, Crowne, and Smith 1977, Savage, Browne, and Bolton 1976, Wills and Wills 1976, and Hewitt and Burbidge 1980.

[c] The optical identifications are mainly from McEwan, Browne, and Crowther 1975, with the rest coming from Veron *et al.* 1976, Veron and Veron 1977, Wall, Shimmins, and Merkelijn 1971, Wills and Lynds 1978, Hewitt and Burbidge 1980, and Kuhr 1979. Optical identification codes: Q = quasar, G = galaxy, E (E0, E1, E2, E3, E4) = elliptical galaxy (types 0–4), NG = N galaxy, N2 = N2 galaxy, D = diffuse galaxy, CG = compact galaxy, EF = empty field, U = unidentified.

[d] Optical magnitudes are from McEwan, Browne, and Crowther 1975.

[e] Optical color is from McEwan, Browne, and Crowther 1975 and is the difference between their estimated Palomar blue and red magnitudes.

[f] Radio variability is from Savage, Jauncey, and Wright 1983.

[g] The angular sizes of extended radio structure are from McEwan, Browne, and Crowther 1975 and Wills 1979.

[h] Experiment codes: A = 1977 February 20, B = 1977 February 21, C = 1977 February 23, D = 1977 February 25, E = 1977 April 21, F = 1977 April 22, G = 1977 December 13.

[i] Fringe visibility is defined as the correlated flux density divided by the total flux density.

galaxies at 8095 MHz with a detection limit an order of magnitude smaller than ours. We are presently searching for milli-arcsecond cores in a complete sample of radio galaxies with an order of magnitude more sensitivity than our present study.

b) The Existence of Milli-Arcsecond Cores as a Function of the Fraction of the Source Power Emanating from the Core

Does a milli-arcsecond source exist at the core of all extragalactic radio sources? We examine this question in Figure 1, which plots the percentage of sources display-ing milli-arcsecond cores as a function of fringe visibility. It should be kept in mind that we have observed each source at only a single (u, v)-point. Hence, for each source, the observed correlated flux density repre-sents the minimum flux density that could be emanating from the milli-arcsecond structure.

Figure 1 shows results for both the entire sample and for quasars only. Similar plots on the visibility behavior of galaxies and empty fields must await more sensitive observations. In this figure we have taken into account that the effective sample size for visibility values less than 0.3 is smaller than our full sample size because of our limited sensitivity. The minimum effective sample

TABLE 2

THE DISTRIBUTION OF DETECTED AND UNDETECTED
MILLI-ARCSECOND COMPONENTS AS A
FUNCTION OF OPTICAL IDENTIFICATION

Optical Identification	Number Detected	Number Not Detected
Q	25	7
G	1	10
E	0	1
E0	0	2
E1	0	2
E2	0	2
E3	1	0
E4	0	2
D	0	2
CG	0	2
NG	1	1
N2	0	2
EF	7	31
U	1	3
Total	36	67

NOTE.—For abbreviations see Table 1, note c.

size used in an individual visibility bin is 18 sources. Since Figure 1 represents only limited numbers of detections, high uncertainty exists in the percentages shown, but the indicated trends are clearly significant. These trends show that for both the entire sample and for quasars alone, the percentage of sources displaying milli-arcsecond cores increases with increasing rate as the fringe visibility detection limit is lowered. In each case a majority of the sources display milli-arcsecond cores above a visibility of 0.05. In particular, the nature of the quasar plot suggests that all the quasars will show milli-arcsecond cores when higher sensitivity observations are completed. The relationship between the fraction of source flux density in a milli-arcsecond nucleus and the overall radio structure can provide constraints on models of the nature and evolution of the radio emission for both quasars and galaxies.

Virtually all of the sources observed appear to be at least partially resolved indicating that a measurable portion of each source's flux is emanating from components larger than ~ 0.5 milli-arcsec. The mean visibility for detected quasars is 0.39, for detected galaxies 0.10, and for detected empty fields 0.44. There are two possible contributing factors to most sources being partially resolved. First, the radio spectra of the sources suggest that single-component sources are rare. This is supported by Broderick and Condon's (1975) finding that none of their 100 sources were completely unresolved with angular resolution 20 times poorer than ours. Second, as the range of brightness temperature sampled by our Australia-California interferometer is near the ~ 10^{12} K Compton limit (Kellermann and Pauliny-Toth 1969), even the smallest components may be partially resolved

on this baseline. We note that the Broderick and Condon study did not approach the Compton limit.

c) Relationship to Larger Radio Structure

All 103 sources in our sample have previously been searched for radio structure larger than ~ 10″ in extent; 46 have been identified as possessing such radio structure. Almost all of the galaxies in the sample show large structure, while only about 25% of the quasars do. The large angular size quasars seem to display a much higher probability of possessing a detectable milli-arcsecond core (4 of 8 do) than do the large angular size galaxies (3 of 23 do). Of the extended quasars, the four with detected cores are all smaller in overall extent than the four with no detected cores. On the other hand, the three galaxies with detected VLBI cores are among the galaxies with largest structure.

d) Correlation with Radio Spectral Index and Radio Variability

Figure 2a shows the relationship between the existence of milli-arcsecond cores and radio spectral index. In general, the less steep the radio spectrum, the more likely the existence of a detectable milli-arcsecond core and the higher the percentage of source flux density found to be coming from such cores. This behavior is consonant with the generally accepted theory of synchrotron self-absorption domination of the core emission. We note the sharp correlation between both the
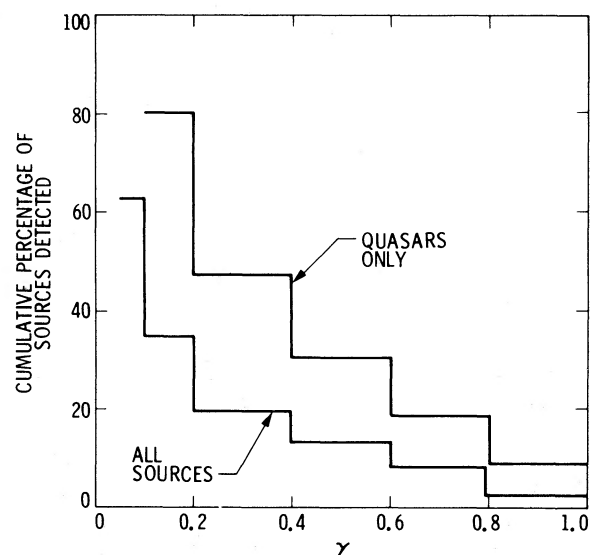
FIG. 1.—Percentage of sources found to possess a milli-arcsecond core as a function of fringe visibility (γ). Corrections have been applied for decreasing effective sample size at low visibilities owing to limited sensitivity. The solid lines show the cumulative percentage of the sample detected as the visibility detection limit is lowered.
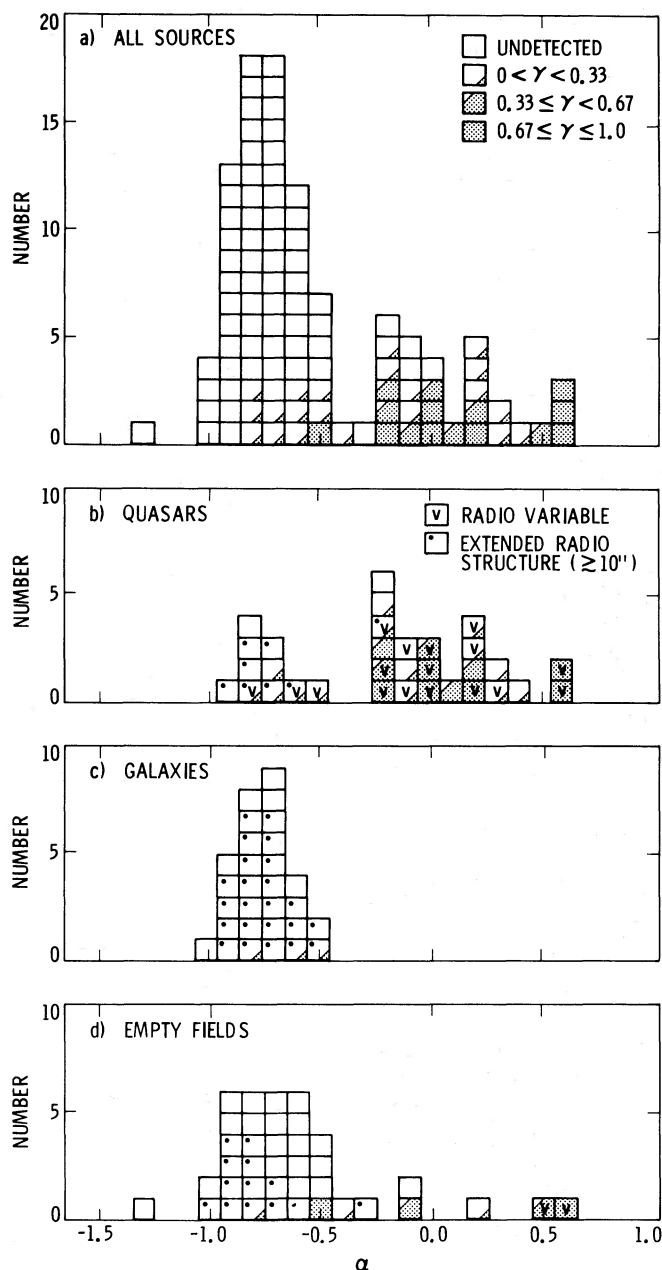
FIG. 2.—The detection of milli-arcsecond cores as a function of radio spectral index and optical identification. Degree of shading of each box indicates fringe visibility (γ). Radio variability and extended radio structure are also denoted.

detection rate and the detected fringe visibility of the milli-arcsecond cores and the two lobes of the bimodal spectral index distribution (Wall 1972b; Condon and Jauncey 1974). In the flat spectrum lobe almost all sources display milli-arcsecond structure, and a significant fraction of the sources have high fringe visibilities. Although this lobe spans a wide spectral index range from -0.2 to $+0.6$, there is no strong trend toward higher fringe visibilities from one edge of the lobe to the other. In the steep spectrum lobe, only a small fraction of the sources (15%) show milli-arcsecond structure. The detected sources in this lobe almost all display low visibilities and are all grouped toward the flatter spectral index side of the lobe.

Figures 2b, 2c, and 2d show a breakdown of the spectral index histogram into the three major optical identification categories. The quasars display the previously noted bimodal distribution in spectral index, while

the galaxies exclusively occupy the steep spectrum lobe of the distribution, and empty field sources are mainly in the steep spectrum lobe. The empty field distribution is consistent with Wall's (1972 b) estimate that 25% ± 10% of the empty field sources are quasars, and the rest, galaxies. The quasars exhibit the bimodal distribution of detection rate and detected fringe visibility previously described. Quasars occupying the steep spectrum lobe of the bimodal spectral index distribution seem more likely to possess a detectable milli-arcsecond core than do the galaxies and empty field sources in the steep spectrum lobe; 50% (5 of 10) of the quasars in the steep spectrum lobe display a milli-arcsecond core, while only 10% (3 of 29) of the galaxies and 10% (3 of 32) of the empty field sources in the steep spectrum lobe display a milli-arcsecond core. Based on the relative detection rate of milli-arcsecond cores, the probability that the quasars and galaxies in the steep spectrum lobe belong to the same population is less than 3%. Because of the small sample sizes, the statistical test used here and in later sections includes a continuity correction (Kendall and Stuart 1946).

Flux density measurements at 2.7 and 5.0 GHz of the entire Parkes 4° catalog have been made at three epochs spanning a decade (Savage, Jauncey, and Wright 1983), providing an indication of the stronger radio variables (noted in Table 1). Figures 2b, 2c, and 2d show that radio variability is strongly correlated with the detection rate and detected fringe visibility of milli-arcsecond cores. Only two of the variable sources do not have a detected milli-arcsecond core: 1351+021 (Q), and 1635 −035 (U). Both of these sources have decreased to a total flux density of ∼ 0.4 Jy at 2.7 GHz and would have had detected milli-arcsecond cores only if their fringe visibilities were ≥ 0.3. Of the eight detected sources with fringe visibilities ≥ 0.67, seven are noted variables. 64% of the quasars in the flat spectral index lobe are variable, while only 30% of the quasars in the steep spectrum lobe and none of the galaxies are.

Figures 2b, 2c, and 2d also show that those sources with extended radio structure tend to fall almost exclusively in the steep spectral index lobe and tend not to show milli-arcsecond cores. No source with extended structure has a fringe visibility greater than 0.2. The fact

that a higher percentage of steep spectrum quasars in our sample possess a detectable milli-arcsecond core than do steep spectrum galaxies is undoubtedly related to the previous observation that a higher percentage of large-structure quasars possess a detectable milli-arcsecond core than do large-structure galaxies. We also note that extended radio structure among empty field sources seems .to be much less common than might be predicted if 75% ± 10% of these sources are galaxies (only 35% show extended structure).

e) Correlation with Redshift

Of the quasars in our sample, 24 have known redshifts, 18 of which have detected milli-arcsecond cores. Since redshifts are known for only seven of the galaxies, we have no clues to the redshift behavior of their milli-arcsecond cores. Figure 3 shows the relationship between the detection of milli-arcsecond cores in quasars and redshift. Over the redshift range of the quasars ($0.15 < z < 2.6$), there is no evidence for any redshift dependence of the probability that a quasar will possess a detectable milli-arcsecond core or of the fringe visibility of the detected cores. Although the sample is small, strong correlations would probably have been evident. The strong correlation previously noted between quasar milli-arcsecond structure and lobe membership in the bimodal spectral index distribution does not manifest itself in the redshift distribution because of the spreading of sources from both lobes across much of the redshift range. The measured fringe visibilities depend on both the fraction f of the source brightness contained in a compact component and the angular size θ of that component. The implied independence of fringe visibility and redshift probably indicates that neither f nor θ depends strongly on redshift.

To interpret angular size in terms of intrinsic linear size of a source, we employ the Robertson-Walker metric. The cosmological (luminosity) distance of a source is

$$R = c(1+z)^{-1}(H_0 q_0^2)^{-1}$$

$$\times \left[q_0 z - (q_0 - 1)\left(1 - \sqrt{2 q_0 z + 1}\right)\right] \text{ Mpc,}$$
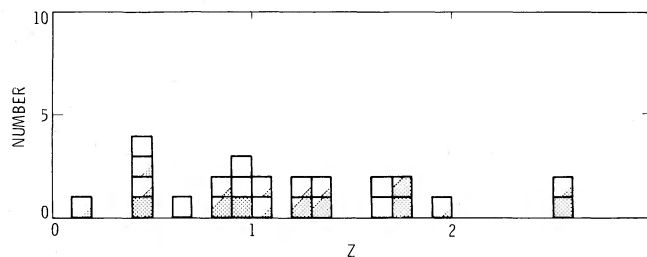
Fig. 3.—The detection of milli-arcsecond cores in quasars as a function of redshift. Degree of shading of each box indicates fringe visibility (γ) as in Fig. 2.

where H_0 is the Hubble constant (assumed to be 55 km s^{-1} Mpc^{-1}), and q_0 is the deceleration parameter. Source linear size, X, is then given by $X = R\theta(1 + z)^{-1}$ Mpc, where θ is the angular source size in radians. Figure 4 displays X corresponding to $\theta = 1$ milli-arcsec as a function of redshift for a set of possible values of q_0. We see that the linear source size equivalent of 1 milli-arcsec is reasonably insensitive to redshift for each value of the deceleration parameter over most of the redshift range of our quasar sample $(0.15 < z < 2.6)$. Hence, the failure to detect a strong correlation between the VLBI angular structure of quasars and redshift could perhaps be interpreted as the lack of a strong evolution in linear size for the compact cores of radio quasars.

Other investigators have tried to utilize the relationship between radio source angular size and redshift as a probe of quasar evolution and cosmology. Previous results suggest that large-scale quasar angular size is independent of redshift (Riley, Longair, and Hooley 1977; Wardle and Potash 1977; Masson 1980). This is in contrast to samples which include both galaxies and quasars, in which the large-scale angular size is found to be approximately proportional to z^{-1} (cf. Ekers and Miley 1977; Riley, Longair, and Hooley 1977). In addition, the angular sizes of radio hot spots that are found near the outer extremities of powerful double sources have been measured by scintillation techniques, and the hot spot angular sizes appeared to be substantially independent of redshift for a sample which was dominated by quasars (Hewish, Readhead, and Duffett-Smith 1974). Since our results suggest the angular sizes of the milli-arcsecond radio cores in quasars do not depend strongly on redshift, there is evidence on three different size scales and for three different quasar structural components that radio quasar angular size, and perhaps linear size, is independent of redshift.

f) Radio Luminosity of the Milli-Arcsecond Cores

The radio luminosity of the milli-arcsecond cores may be calculated from $L = 4\pi R^2(1 + z)(10^{-26}S_c)$ watts Hz^{-1}, where S_c is the detected correlated flux density in janskys and R is in meters. This equation assumes that the source nucleus is unresolved and that it is radiating isotropically. The true source luminosity could be significantly less than the calculated value if we assume the radiation to be beamed toward the observer. The deceleration parameter was chosen to be 0.5. Luminosities were calculated for sources with known redshift and refer to the emitted frequency in the rest frame of the source.

Figure 5 shows the distribution of sources as a function of the radio luminosity of the milli-arcsecond core. The distribution divides into separate but contiguous populations of galaxies and quasars, with luminosities and luminosity upper limits being bounded by
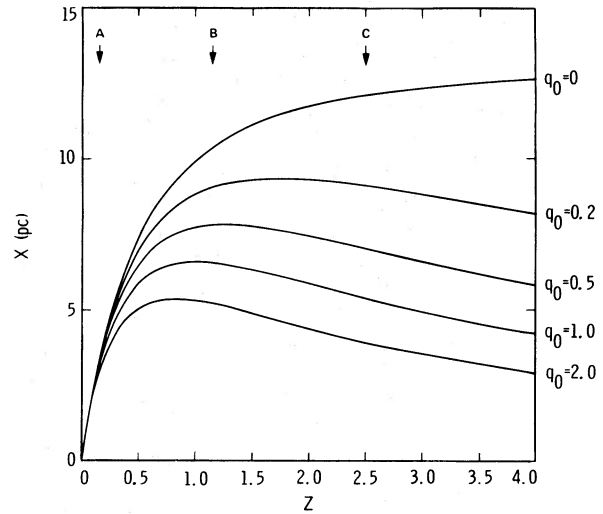
FIG. 4.—Linear source size (X) corresponding to a constant angular source size of 10^{-3} arcsec as a function of redshift (z) and deceleration parameter (q_0). Significant redshift values within quasar sample are noted as follows: A = minimum z (i.e., with measured z), B = mean z, C = maximum z.

$\sim 10^{24} - \sim 10^{26}$ watts Hz^{-1} for galaxies and $\sim 10^{26} - \sim 10^{28}$ watts Hz^{-1} for quasars. The largest value of detected quasar core luminosity exceeds the largest value of galaxy core luminosity by a factor of about $\sim 4 \times 10^2$. For the quasars alone, we note no significant dependence of fringe visibility on the total radio luminosity (watts Hz^{-1}) of each source.

g) Radio Brightness Temperatures

Figure 6 shows the distribution of radio brightness temperatures of the detected sources. The brightness temperatures of the sources were calculated by assuming the source brightness distributions to be Gaussian, and have not been multiplied by $(1 + z)^{-1}$ to correct to the rest frame of the source, which would decrease the displayed sample size. The brightness temperatures range between $\sim 3 \times 10^{10}$ K and $\sim 6 \times 10^{12}$ K. These results are consistent with the Compton limit of $\sim 10^{12}$ K. However, brightness temperatures much in excess of 10^{12} K are not measurable with baselines that are less than an Earth-diameter in length.

h) Correlation with Optical Magnitude

Figure 7 shows the distribution of quasars as a function of optical magnitude. Apparent optical magnitudes existed for all optically identified quasars in our sample. Again, the small number of detected galaxies prohibits any conclusions to be drawn about the galaxies. The magnitudes have not been corrected for absorption or redshift. No obvious trend exists in the rate of detection of milli-arcsecond cores in quasars as a function of
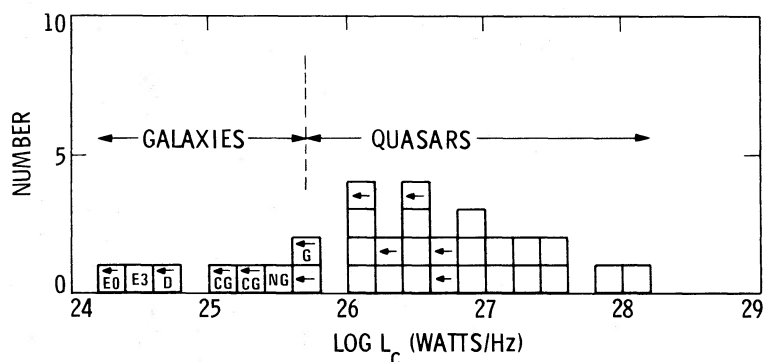
FIG. 5.—Distribution of sources as a function of the radio luminosity (L_c) of the compact core. Optical identification is denoted. Unlettered boxes are quasars. Boxes with arrows show upper limits.
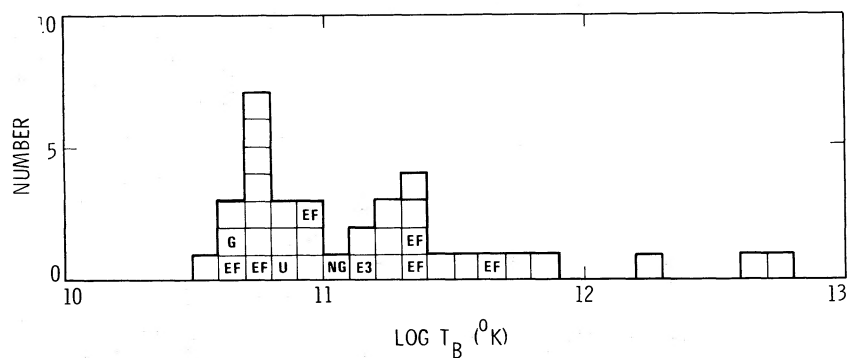
FIG. 6.—The distribution of brightness temperatures (T_B) of detected milli-arcsecond cores. Optical identifications are shown, with unlettered boxes denoting quasars.
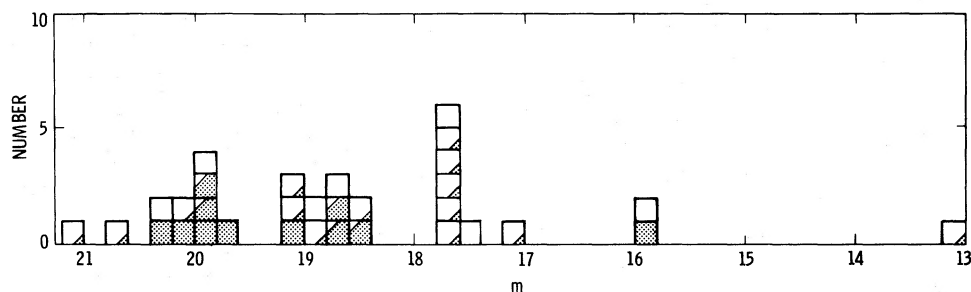
FIG. 7.—Distribution of quasars as a function of optical magnitude. Fringe visibility is denoted as in previous figures.

optical magnitude. However, there is a marginally significant trend at the 7% level toward a higher percentage of the flux density of a source emanating from a milli-arcsecond core as optical brightness decreases. For quasars with optical magnitudes < 18, only one of 11 quasars displays a fringe visibility ≥ 0.33, while for quasars with optical magnitudes > 18, 10 out of 21 display fringe visibilities ≥ 0.33.

Figure 8 shows the behavior of correlated flux density versus optical magnitude for detected sources. This plot allows direct comparison of the source optical luminosity and the radio luminosity of the compact core. No definitive correlation is apparent in this plot. We note that Condon, Balonek, and Jauncey (1976) have speculated that high radio luminosity of compact radio cores is correlated with high optical luminosity of radio
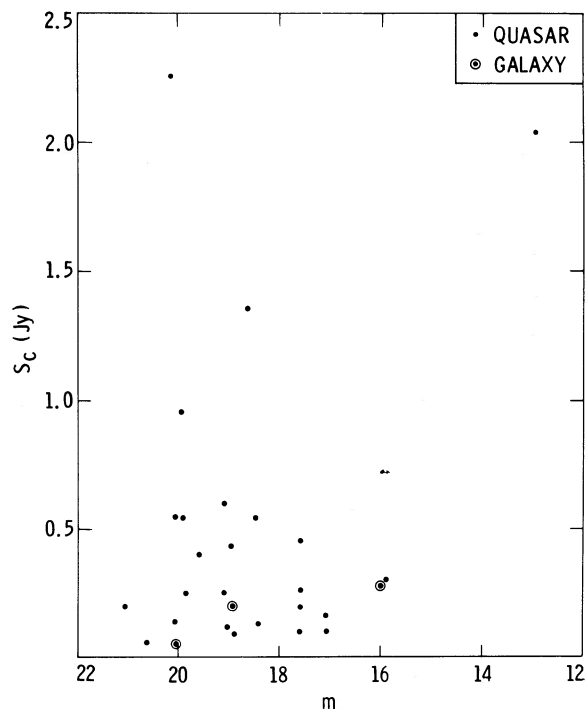
FIG. 8.—Correlated flux density (S_c) vs. apparent optical magnitude for detected sources.

FIG. 9.—Distribution of quasars as a function of optical color. Optical color shown is Palomar blue minus Palomar red. Fringe visibility is denoted as in previous figures.

sources. This trend does not appear readily evident for milli-arcsecond radio cores.

i) Correlation with Optical Color

Figure 9 shows the distribution of quasars as a function of optical color. The color estimates taken from Table 1 are Palomar blue minus Palomar red magnitude estimates from McEwan, Browne, and Crowther (1975). These magnitudes have been measured for all but two of the identified quasars ($B - V$ colors exist only for a smaller fraction of the sample). Toward the red end of the quasar population, there is a significant trend at the 1% level toward a larger fraction of the flux density of the source emanating from a milli-arcsecond core. For quasars with colors of 0.4 mag or bluer, only two out of 16 have fringe visibilities ≥ 0.33, while for quasars with colors of 0.5 mag or redder, nine out of 14 have fringe visibilities ≥ 0.33. A similar though less significant trend appears with the smaller sample for which published $B - V$ colors exist. However, the trend is not apparent in a comparison with the published $U - B$ colors.

It is interesting to note that BL Lacertae objects and optically violent variables (OVV) have generally redder $B - V$ colors than do quasars. They are also often more rapid variables than quasars, suggesting that their emitting regions are smaller.

If the general correlation between compactness and color is real, it can perhaps be explained by the model of

continuum emission in quasars presented by Marscher (1980). In this model, the continuum emission of quasars comes from two distinct regions, the relativistic jets and the central "energy machine." When the jets are nearly aligned with the observer, the observed compact radio flux increases, and the jets dominate the optical emission and cause the observer to measure a much steeper optical spectrum than might be expected from the jet electron energy spectrum. This is due to inhomogeneities in magnetic field, electron density, and electron energy within the jet. However, when the angle between the jets and the observer is large, the contributions from the jets and the central source are more comparable, and the combined optical spectrum is not as steep as that of the observer-directed jet. Hence, we might speculate that the more end-on we view the jets, the redder the optical spectrum, and the stronger or more compact the VLBI radio component.

IV. SUMMARY

Milli-arcsecond radio nuclei were found in 36 sources out of a radio complete sample of 103 extragalactic sources. We have studied the statistical relationship of the milli-arcsecond cores to other source properties, both radio and optical, but the relationships that were found were in many cases only tentative owing to the limitations of the data.

We examined both the convincing and tentative relationships in light of a currently popular theoretical model of extragalactic radio sources in which compact energetic nuclei eject relativistic jets that supply energy to the more extended source components. This theory might be argued to be consistent with the observations that most if not all bright radio quasars possess a milli-arcsecond core and that a trend exists toward higher fringe visibility of milli-arcsecond quasar cores toward the red end of the optical spectral distribution. The decreasing relative abundance of detected milli-arcsecond cores as we pass from quasars without extended structure to quasars with extended structure to galaxies could be viewed as an evolutionary trend toward decreasing core prominence, perhaps due to a decrease in the flow of matter (and hence energy) into

the nucleus or due to a spin-down of a central black hole as suggested by Meier (1983). In addition, the synchrotron self-absorbed model for the radiation from the milli-arcsecond cores is consistent with the observations that the detectability and fringe visibility of the milli-arcsecond cores are correlated with the radio spectral index and variability of the source. The observation that virtually all sources were partially resolved could be a result of approaching the Compton brightness temperature limit of synchrotron self-absorbed radiation.

It was also noted that quasars with steep radio spectra are perhaps more likely to possess a stronger milli-arcsecond core than are galaxies with equally steep spectra and that there is a marginally significant trend toward quasar radio compactness as observed optical brightness decreases. The absence of a strong correlation between quasar milli-arcsecond structure and redshift was interpreted as possible evidence of a lack of strong physical evolution in quasars, a hypothesis which is in agreement with previous studies of the size evolution of both quasar large-scale radio structure and radio lobe hot spots.

Statistical studies of the milli-arcsecond nuclei of extragalactic radio sources should be pursued with larger sample sizes, greater sensitivity, and more complete structure information. Such investigations could be important not only in unraveling the nature of the compact radio cores, but also for possible cosmological tests.

REFERENCES

Blandford, R. D., and Rees, M. J. 1974, *M.N.R.A.S.*, **169**, 395.
Broderick, J. J., and Condon, J. J. 1975, *Ap. J.*, **202**, 596.
Burbidge, G. R., Crowne, A. H., and Smith, H. E. 1977, *Ap. J. Suppl.*, **33**, 113.
Clark, B. G. 1973, *Proc. IEEE*, **61**, 1242.
Condon, J. J., Balonek, T. J., and Jauncey, D. L. 1976, *A.J.*, **81**, 913.
Condon, J. J., and Jauncey, D. L. 1974, *A.J.*, **79**, 437.
Ekers, R. D., and Miley, G. K. 1977, in *IAU Symposium 74, Radio Astronomy and Cosmology*, ed. D. L. Jauncey (Dordrecht: Reidel), p. 109.
Hewish, A., Readhead, A. C. S., and Duffett-Smith, P. 1974, *Nature*, **252**, 657.
Hewitt, A., and Burbidge, G. 1980, *Ap. J. Suppl.*, **43**, 57.
Kellermann, K. I., and Pauliny-Toth, I. I. K. 1969, *Ap. J. (Letters)*, **155**, L71.
Kendall, M. G., and Stuart, A. 1946, *The Advanced Theory of Statistics*, Vol. II (London: Griffin and Co.), p. 555.
Klein, M. J., and Stelzreid, C. T. 1976, *A.J.*, **81**, 1078.
Kuhr, H. 1979, Max-Planck-Institute, preprint No. 55.
Marscher, A. P. 1980, *Ap. J.*, **235**, 386.
Masson, C. R. 1980, *Ap. J.*, **242**, 8.
McEwan, N. J., Browne, I. W. A., and Crowther, J. H. 1975, *M.N.R.A.S.*, **80**, 1.
Meier, D. L. 1983, in preparation.
Pearson, T. J., and Readhead, A. C. S. 1981, *Ap. J.*, **248**, 61.

Readhead, A. C. S., Cohen, M. H., and Blandford, R. D. 1978, *Nature*, **272**, 131.
Riley, J. M., Longair, M. S., and Hooley, A. 1977, in *IAU Symposium 74, Radio Astronomy and Cosmology*, ed. D. L. Jauncey (Dordrecht: Reidel), p. 133.
Savage, A., Browne, I. W. A., and Bolton, J. G. 1976, *M.N.R.A.S.*, **177**, 77.
Savage, A., Jauncey, D. L., and Wright, A. E. 1983, in preparation.
Schilizzi, R. T. 1976, *A.J.*, **81**, 946.
Speed, B., and Warwick, R. S. 1978, *M.N.R.A.S.*, **182**, 761.
Ulvestad, J., Johnston, K., Perley, R., and Fomalont, E. 1981, *A.J.*, **86**, 1010.
Veron, M. P., and Veron P. 1977, *Astr. Ap. Suppl.*, **29**, 149.
Veron, M. P., Veron, P., Adgie, R. L., and Gent H. 1976, *Astr. Ap.*, **47**, 401.
Wall, J. V. 1972a, *Australian J. Phys., Ap. Suppl.*, **24**, 1.
——. 1972b, *Australian J. Phys., Ap. Suppl.*, **24**, 49.
Wall, J. V., Shimmins, A. J., Merkelijn, K. 1971, *Australian J. Phys., Ap. Suppl.*, **19**, 1.
Wardle, J. F. C., and Potash, R. 1977, in *IAU Symposium 74, Radio Astronomy and Cosmology*, ed. D. L. Jauncey (Dordrecht: Reidel), p. 137.
Wills, D. 1979, *Ap. J.*, **39**, 291.
Wills, D., and Lynds, R. 1978, *Ap. J. Suppl.*, **36**, 317.
Wills, D., and Wills, B. J. 1976, *Ap. J. Suppl.*, **31**, 143.
Yerbury, M. J. 1975, *Rev. Sci. Instr.*, **46**, 169.

DAVID L. JAUNCEY: CSIRO, Division of Radiophysics, c/o Division of Soils, P.O. Box 639, Canberra City, A.C.T. 2601, Australia

DAVID D. MORABITO and ROBERT A. PRESTON: 264-781, Jet Propulsion Laboratory, 4800 Oak Grove Drive, Pasadena, CA 91109